BI 6727, A Polo-like Kinase Inhibitor with Improved Pharmacokinetic Profile and Broad Antitumor Activity

Dorothea Rudolph,[1] Martin Steegmaier,[1] Matthias Hoffmann,[2] Matthias Grauert,[2] Anke Baum,[1] Jens Quant,[1] Christian Haslinger,[1] Pilar Garin-Chesa,[1] and Günther R. Adolf[1]

Abstract

Purpose: Antimitotic chemotherapy remains a cornerstone of multimodality treatment for locally advanced and metastatic cancers. To identify novel mitosis-specific agents with higher selectivity than approved tubulin-binding agents (taxanes, *Vinca* alkaloids), we have generated inhibitors of Polo-like kinase 1, a target that functions predominantly in mitosis.

Experimental Design: The first compound in this series, suitable for i.v. administration, has entered clinical development. To fully explore the potential of Polo-like kinase 1 inhibition in oncology, we have profiled additional compounds and now describe a novel clinical candidate.

Results: BI 6727 is a highly potent (enzyme IC_{50} = 0.87 nmol/L, EC_{50} = 11-37 nmol/L on a panel of cancer cell lines) and selective dihydropteridinone with distinct properties. First, BI 6727 has a pharmacokinetic profile favoring sustained exposure of tumor tissues with a high volume of distribution and a long terminal half-life in mice (V_{ss} = 7.6 L/kg, $t_{1/2}$ = 46 h) and rats (V_{ss} = 22 L/kg, $t_{1/2}$ = 54 h). Second, BI 6727 has physicochemical and pharmacokinetic properties that allow *in vivo* testing of i.v. as well as oral formulations, adding flexibility to dosing schedules. Finally, BI 6727 shows marked antitumor activity in multiple cancer models, including a model of taxane-resistant colorectal cancer. With oral and i.v. routes of administration, the total weekly dose of BI 6727 is most relevant for efficacy, supporting the use of a variety of well-tolerated dosing schedules.

Conclusion: These findings warrant further investigation of BI 6727 as a tailored antimitotic agent; clinical studies have been initiated.

In eukaryotes from yeast to men, orthologues of Polo-like kinase 1 (Plk1) control multiple essential steps of mitosis (reviewed in refs. 1, 2). In vertebrate cells, Plk1 has been implicated in the activation of Cdk1-cyclin B at mitotic entry (3), centrosome maturation (4), release of cohesin from chromosome arms (5), formation and maintenance of the bipolar spindle (6–8), mitotic exit (9), and cytokinesis (7, 10–13). In addition, Plk1 is a target of the DNA damage checkpoint (14, 15) and seems to be required for mitotic reentry after DNA damage checkpoint recovery (16). Plk1 mRNA and protein expression, its catalytic activity, and subcellular localization are tightly regulated during cell cycle progression (17). Plk1 is located at centrosomes and kinetochores during early mitosis, and a fraction translocates to the midzone/midbody late in mitosis (18). Based on its temporal and spatial expression patterns as well as genetic and biological evidence, Plk1 seems to function uniquely in the regulation of the cell division cycle during late G_2 and M phases. In previous studies, we have used small interfering RNA (siRNA) and a chemical biology approach with BI 2536 (6, 8, 13, 19) to validate this role of Plk1 in human cells. We observed that the cellular effects of down-regulating Plk1 mRNA and protein with siRNA are identical to selective inhibition of its serine/threonine kinase activity. Cellular effects of Plk1 inhibition include a distinctive "polo arrest" phenotype in prometaphase, accumulation of phospho–histone H3, and formation of aberrant mitotic spindles followed by a surge in apoptosis (6). Using BI 2536, these cellular phenotypes in tissue culture were linked to identical effects *in vivo* (19). Of note, three additional Polo-like kinase family members (Plk2/Snk, Plk3/Fnk, and Plk4/SAK) have been identified, but these are thought to function during the G_1 and S phases of the cell cycle (reviewed in ref. 17) and their inhibition apparently does not contribute to the BI 2536–induced cellular phenotype.

Consistent with its biological role, Plk1 mRNA and protein are highly expressed in proliferating tissues and Plk1 seems to be overexpressed in a broad spectrum of cancers, with highest expression levels being correlated with poor prognosis in several cancer types (20). Taken together, these observations highlight Plk1 as an attractive molecular target for the antimitotic approach to cancer therapy (21). Clearly, in this category of antiproliferative agents, the approved tubulin-binding taxanes and *Vinca* alkaloids serve as reference points for clinical efficacy, side effects, and convenience of drug administration. Three lines of continued drug development can be discerned. First, efforts are made to improve the formulation of existing microtubule-stabilizing (taxanes) and destabilizing (*Vinca* alkaloids) drugs, to develop close analogues suitable for

Authors' Affiliations: [1]Boehringer Ingelheim RCV GmbH & Co KG, Vienna, Austria and [2]Boehringer Ingelheim Pharma GmbH & Co KG, Biberach, Germany

Received 9/22/08; revised 1/19/09; accepted 1/20/09; published OnlineFirst 4/21/09.

Requests for reprints: Dorothea Rudolph, Department of Pharmacology, Boehringer Ingelheim RCV GmbH & Co KG, Dr. Boehringer-Gasse 5-11, A-1121 Vienna, Austria. Phone: 43-1-801-052780; Fax: 43-1-801-052366; E-mail: dorothea.rudolph@boehringer-ingelheim.com.

doi:10.1158/1078-0432.CCR-08-2445

Translational Relevance

This article describes the preclinical profile of a novel drug candidate, BI 6727, that is currently in early clinical development. Although classic antimitotic agents such as tubulin binders (e.g., taxanes and *Vinca* alkaloids) are established treatment modalities in cancer therapy, some of their limitations are based on effects on microtubule function in interphase cells. Here, we present preclinical results (pharmacologic profile *in vitro*, pharmacokinetics in rodents, and efficacy in cancer xenograft models) for a novel small-molecule inhibitor of Polo-like kinase 1 (Plk1), a new target for cancer therapy. Plk1 regulates multiple steps in mitosis. Inhibition of Plk1 predominantly affects dividing cells and potentially avoids some of the side effects observed with classic tubulin-binding drugs.

oral administration, and to develop novel chemical series of antimicrotubule agents, like epothilones, to overcome taxane resistance (22). Second, mitotic kinesins have been identified as microtubule-associated motor proteins and ATPases like Eg5 or CENP-E represent novel drug targets that provide specificity for the cell division–related function of microtubules (23, 24). Finally, the cell cycle–regulatory kinases CDK1, Aurora B, and Plk1 are tubulin-independent targets for mitotic inhibitors that are readily accessible to medicinal chemistry approaches (25).

Of these three potential mitotic kinase targets, Aurora B has thus far been targeted extensively by drug candidates. The results of the first clinical trials with these Aurora B inhibitors are pending (26). Plk1 inhibitors have emerged more recently (7, 19, 27–29) with BI 2536 as the first compound to enter clinical studies. ON01910 has been reported earlier to act via Plk1 (30), but this notion was not corroborated in subsequent studies (6, 29) and its mode of action remains to be defined. While the first clinical studies of Plk1 inhibitors are ongoing, we and others (7, 19, 27–29) are continuing to broaden the range of clinical candidates targeting Plk1. These efforts are aided by the lessons learned from our previous program on the chemical optimization of dihydropteridinones and emerging X-ray crystallographic data regarding the basis of high Plk1 kinase selectivity (31, 32).

Here, we report on BI 6727, a dihydropteridinone derivative with high potency and selectivity. In preclinical studies, a high volume of distribution, indicating good tissue penetration, and a long terminal half-life have emerged as distinct features of BI 6727, which may have a favorable effect on antitumor efficacy *in vivo*. The results of ongoing clinical studies in cancer patients will allow a comparison with human pharmacokinetic and pharmacodynamic parameters in the future.

Materials and Methods

Chemistry. The dihydropteridinone BI 6727 was derived from a chemical lead optimization program designed to generate Plk inhibitors (Patent Application WO 2004/076454).

Crystal structure. Protein expression of the T210V mutant kinase domain was done using a baculovirus/insect cell expression system. A homogeneity of >95% as judged by Coomassie-stained SDS-PAGE was achieved after a chromatographic purification procedure including affinity, ion exchange, and gel filtration chromatography. Protein crystallization was done using the sitting drop method with a reservoir containing 3% to 16% PEG 3350-6000 and 0.2 to 0.5 mol/L sodium malonate (31). Protein-ligand complexation was done before crystallization by incubation of the ligand for 2 h at 4°C. Crystals were frozen using the Proteros Free Mounting System. Data were collected at the SLS beam line X06SA (Swiss Light Source, Paul Scherrer Institute) using the PILATUS 6M detector. Images were processed with XDS; structure solution was achieved by Patterson search methods and model building; and refinement was done with COOT and REFMAC. Protein crystallography was done by Proteros biostructures GmbH. The structure has been deposited in the Protein Data Bank under the access code 3FC2.

In vitro *kinase assays.* Recombinant human Plk1 (residues 1-603) was expressed as NH_2-terminal, GST-tagged fusion protein using a baculoviral expression system (BaculoGold, BD Biosciences) and purified by affinity chromatography using glutathione-agarose (Amersham Biosciences). NH_2-terminal His_6-tagged recombinant human Plk3 (residues 19-301) was purchased from Upstate Cell Signaling Solutions, whereas recombinant human Plk2 was obtained from Invitrogen. Enzyme activity assays for Plk1, Plk2, and Plk3 were done in the presence of serially diluted inhibitor using 20 ng of recombinant kinase and 10 μg casein from bovine milk (Sigma) as substrate. Kinase reactions were done in a final volume of 60 μL for 45 min at 30°C [15 mmol/L $MgCl_2$, 25 mmol/L MOPS (pH 7.0), 1 mmol/L DTT, 1% DMSO, 7.5 μmol/L ATP, 0.3 μCi γ-^{32}P-ATP]. Reactions were terminated by the addition of 125 μL of ice-cold 5% TCA. After transferring the precipitates to MultiScreen mixed ester cellulose filter plates (Millipore), plates were washed with 1% TCA and quantified radiometrically. Dose-response curves were used for calculating IC_{50} values. To establish a kinase selectivity profile, additional kinase assays were done by contract research organizations or reagents were purchased from commercial sources and assays were done according to the supplier's instructions. Appropriate positive and negative controls were included in the assay design.

Cell culture and proliferation assays. Cancer cell lines were obtained from the American Type Culture Collection or the German National Resource Center for Biological Material and were cultured according to the supplier's instructions. Cell proliferation assays were done by incubating cells in the presence of various concentrations of BI 6727 for 72 h and cell growth was assessed by measuring Alamar blue dye (Serotec) conversion in a fluorescence spectrophotometer. Effective concentrations at which cellular growth was inhibited by 50% (EC_{50}) were extrapolated from the dose-response curve fit.

Cell cycle analysis. Logarithmically growing NCI-H460 cells were incubated with 0.1% DMSO or various concentrations of BI 6727. To determine the DNA content, cell suspensions were fixed in 80% ethanol, treated for 5 min with 0.25% Triton X-100 in PBS, and incubated with 0.1% RNase and 10 μg/mL propidium iodide in PBS for 20 min at room temperature. Cell cycle profiles were determined by flow cytometric analysis (FACSCanto, BD Biosciences).

Immunofluorescence analysis. NCI-H460 cells were plated in four-well chamber slides. The next day, cells were treated for 24 h with various concentrations of BI 6727 or 0.1% DMSO as vehicle control. After fixation and permeabilization of the cells with 4% formaldehyde/Triton X-100 (1:200) for 5 min at room temperature, immunofluorescence staining was done according to standard procedures. Briefly, antitubulin (Sigma T6199) and anti–phospho-histone H3 (Upstate 07-145) antibodies were diluted 1:500 in PBS/2% bovine serum albumin. 4′,6-Diamidino-2-phenylindole dihydrochloride (Roche) was used at a final concentration of 0.05 μg/mL. Cells were mounted in Mowiol and analyzed using a Zeiss Axioplan 2 fluorescence microscope.

Efficacy studies in mice. Female BomTac:NMRI-Foxn1^{nu} mice (Taconic) were grafted s.c. with 2×10^6 HCT 116 human colon carcinoma cells (ATCC CCL-247), 1×10^6 NCI-H460 non–small cell lung cancer cells (ATCC HTB-177), or CXB1 human colon carcinoma

tumor pieces derived from patient material by serial transplantation in nude mice. When tumors had reached a volume of ~50 to 100 mm^3, animals were randomized into treatment and control groups of 10 mice each. BI 6727 was formulated in hydrochloric acid (0.1 N), diluted with 0.9% NaCl, and injected i.v. into the tail vein at the indicated dose and schedule. For oral treatment, BI 6727 was resuspended in 0.5% Natrosol 250 hydroxyethyl-cellulose and given intragastrally via gavage needle. An administration volume of 10 mL per kilogram of body weight was used for both administration routes. Tumor volumes were determined thrice a week using a caliper. The results were converted to tumor volume (mm^3) by the formula length × $width^2$ × $\pi/6$. The weight of the mice was determined as an indicator of tolerability on the same days. Median tumor volumes on the last day of the experiment were used to calculate treated versus control values (= $tumor\ volume_{treated\ mice} \times 100/tumor\ volume_{control\ mice}$).

Immunohistochemistry. For *ex vivo* analysis of histone H3 phosphorylation and apoptosis in tumors, female BomTac:NMRI-$Foxn1^{nu}$ mice were grafted s.c. with 2×10^6 HCT 116 human colon carcinoma cells as described above. The average tumor volume was ~200 mm^3 at the start of the experiment. Tumors were excised from nude mice 6, 24, or 48 h after i.v. administration of a single dose of 40 mg/kg BI 6727 or vehicle control ($n = 3$ per treatment group and time point, total 18 mice) and were processed for immunohistochemistry. In addition, samples from the small and large intestines were obtained at the same time points.

Histone H3 phosphorylation was determined by the avidin-biotin immunoperoxidase method on frozen sections using an antibody to Ser^{10}-phosphorylated histone H3 (Upstate) followed by hematoxylin counterstaining. Apoptosis was quantified with a terminal deoxyribonucleotide transferase–mediated nick-end labeling (TUNEL) assay, using the ApopTag Fluorescein *in situ* apoptosis detection kit (Chemicon International Inc.) and analyzed by fluorescence microscopy.

For image analysis, representative pictures were taken from each tumor with a Zeiss Axiophot microscope at 10× magnification. The mitotic index and the number of apoptotic cells were quantified on digital images using the Definiens Developer image analysis software (Definiens AG). Briefly, the area occupied by the tumor cells arrested in mitosis (pH3-positive cells) was calculated as a percentage of the total "tumor cell area" (#tumor cells + tumor stroma, excluding normal tissues). In addition, the area occupied by apoptotic tumor cells (TUNEL-positive cells) was also calculated as a percentage of the total tumor cell area. The statistical significance was determined by the Student's *t* test.

Pharmacokinetic studies. Female BomTac:NMRI-$Foxn1^{nu}$ mice (Taconic) and male Wistar rats of the strain Crl:WI (Han; Charles

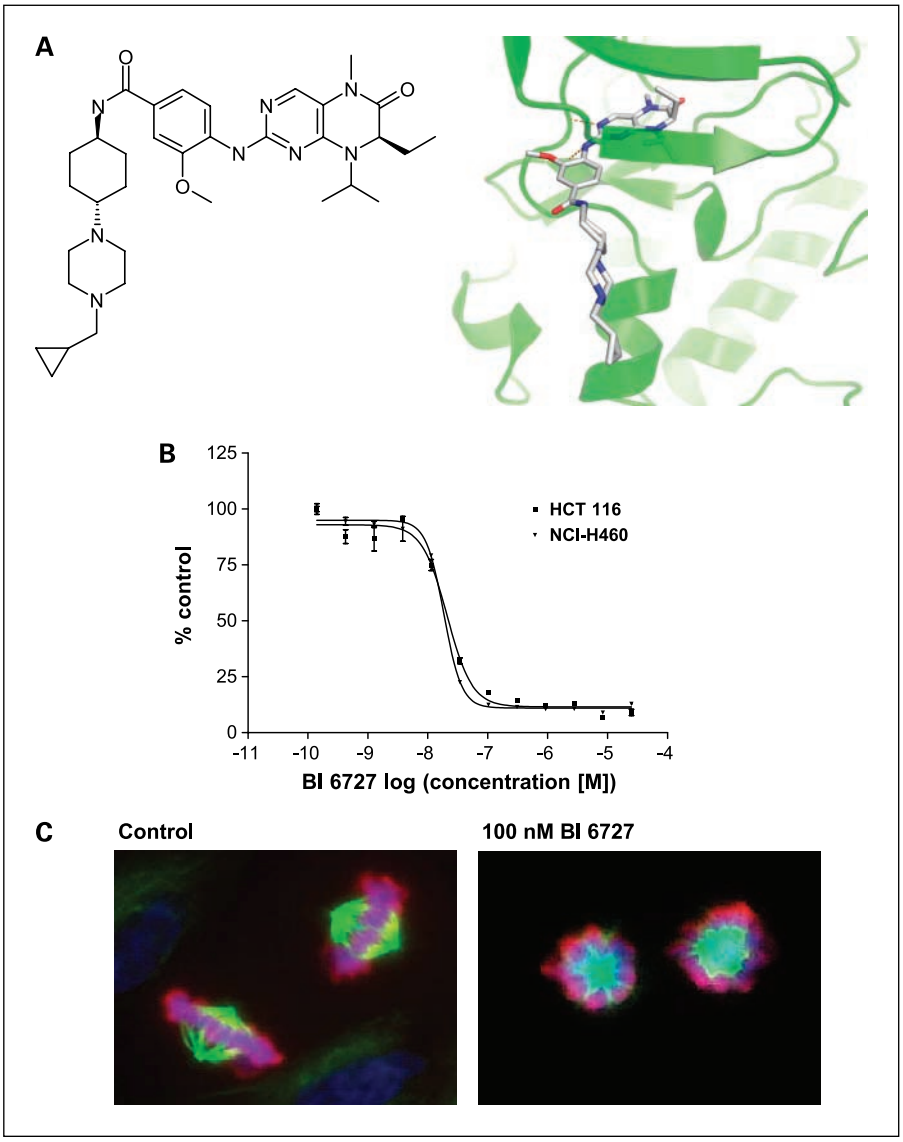

Fig. 1. Chemical structure, X-ray structure, and mode of action of BI 6727. *A,* chemical structure (*left*) and binding mode (*right*) of BI 6727 in the ATP-binding pocket of human Plk1. Orange dotted lines, hydrogen bonds to the backbone atoms of Cys^{133} with distances of 2.8 and 3.1 Å. *B,* Alamar blue–based proliferation assays: dose-response curves of representative experiments using HCT 116 and NCI-H460 cells, respectively. *C,* immunofluorescence analysis of human NCI-H460 non–small cell lung cancer cells treated for 24 h with either 0.1% DMSO (*left*) or 100 nmol/L BI 6727 (*right*) for 24 h. Cells were fixed and stained with 4′,6-diamidino-2-phenylindole (to stain DNA, *blue*) as well as with antitubulin (*green*) and anti–phospho-Ser^{10} histone H3 antibodies (*pink*).

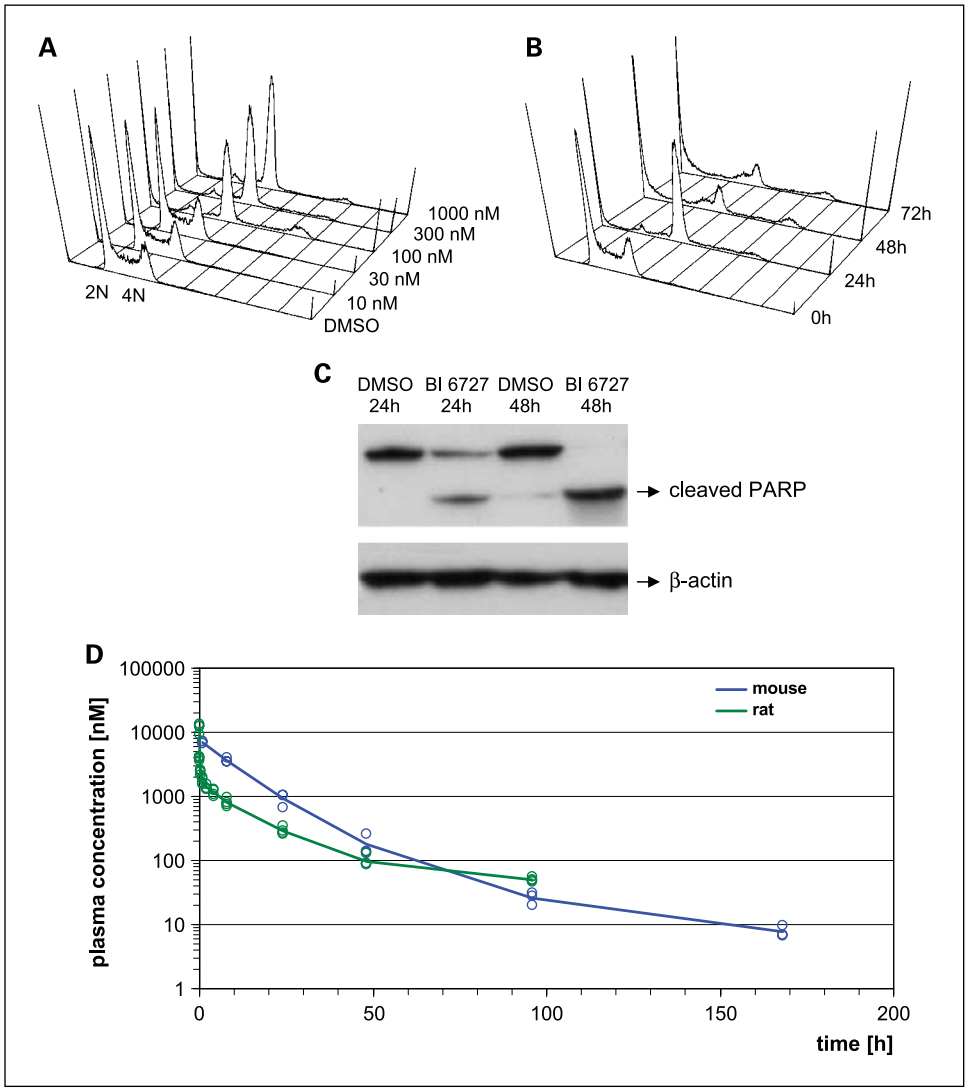

Fig. 2. G_2-M arrest and induction of apoptosis by BI 6727 in NCI-H460 cells. *A,* dose-response experiment: fluorescence-activated cell sorting profile (propidium iodide staining) of exponentially growing NCI-H460 cells treated for 24 h with various concentrations of BI 6727. Starting at a concentration of 100 nmol/L, BI 6727 leads to a prominent G_2-M arrest. Based on our immunofluorescence data, it is clear that the small 8N peak observed reflects cell aggregates rather than binucleated cells. *B,* time course experiment: fluorescence-activated cell sorting profile (propidium iodide staining) of exponentially growing NCI-H460 cells treated for 0, 24, 48, and 72 h with 100 nmol/L of BI 6727. The prominent G_2-M peak observed at 24 h is followed at 48 h by an increase in the sub-G_1 peak, suggesting that G_2-M arrest is followed by the induction of apoptosis. *C,* Western blot analysis of poly (ADP) ribose polymerase (*PARP*) cleavage: Exponentially growing NCI-H460 cells were treated for 24 and 48 h with either DMSO control or 100 nmol/L of BI 6727. Cells were harvested and Western blot analysis for cleaved PARP fragment, a marker of apoptosis, was done. Starting at 24 h, a signal for cleaved PARP fragment is detected, which is even more pronounced at 48 h. *D,* plasma concentration-time profile in rodents after a single dose of BI 6727. BI 6727 was administered i.v. to $n = 4$ rats (10 mg/kg) and $n = 3$ mice (35 mg/kg). Mean values of plasma concentration over time are shown.

River) were used for the pharmacokinetic studies. EDTA plasma was prepared by centrifugation of the collected blood at 10,000 rpm at 4°C. Before analysis, the plasma samples were added to an internal standard and 0.1 N NaOH. The analytes were extracted by liquid-liquid extraction using ethyl acetate. The resulting solution was dried in a warm nitrogen stream and dissolved in 25% methanol/0.1% formic acid.

The tissue samples (100-150 mg) were placed in a 2-mL tube containing Q-Biogene Lysing matrix D (Q-Biogene) and H_2O (6 μL/mg tissue). The mixture was vortexed twice in a Thermo Savant FastPrep FP120 for 30 s at 6.5 m/s. Calibration and quality control samples were added to the analytes after vortexing. Homogenates were diluted 1:1 with 50% methanol/0.1% formic acid containing internal standard for mass spectrometry. Then, acetonitrile was added. After centrifugation for 5 min at 10,000 rpm, the supernatant was used for quantification by liquid chromatography/tandem mass spectrometry.

Quantification of the analytes was done by high-performance liquid chromatography/tandem mass spectrometry (Agilent 1100, Applied Biosystems API3000, ESI+) with a solvent gradient of 95% A to 10% A in 1.5 min [A: 5 mmol/L ammonium acetate (pH 4.0), B: acetonitrile with 0.1% formic acid; Luna C18 3μ 2 × 30].

For the conversion of the tissue concentrations in nmol/mg to nmol/L, a tissue density of 1 was assumed. The area under the curve in the given time interval was calculated from the plasma concentration-time profiles by the trapezoidal rule. Pharmacokinetic parameters were calculated by noncompartmental analysis and terminal half-life was estimated from the last two time points of the concentration-time profile after i.v. administration.

Results

Crystal structure of BI 6727 bound to Plk1. We have screened a diverse library of small molecules for their ability to inhibit the catalytic activity of Plk1 and identified a series of dihydropteridinones that were then further tailored for potency, selectivity, ability to inhibit cell proliferation *in vitro*, and a suitable pharmacokinetic profile. BI 6727 is a derivative of this chemical series (Fig. 1A, *left*); the structure of a cocrystal with the T210V mutant kinase domain of Plk1 (Fig. 1A, *right*) shows a binding mode similar to that previously reported for BI 2536 (32). BI 6727 binds to the hinge region between the NH_2-terminal and COOH-terminal lobes of the kinase domain via two hydrogen bonds from the dihydropteridinone core to the backbone NH and carbonyl group of Cys^{133}. This places BI

Table 1. PK parameters of BI 6727 in rodents

PK parameters	BI 6727	
	Rats	Mice
i.v.		
Dose (mg/kg)	10	35
C_{max} (μmol/L)	11.9	7.1
$AUC_{0\text{-}inf}$ (μmol h/L)	30	100
CL [min/(min kg)]	8.9	10
V_{ss} (L/kg)	22	7.6
$t_{1/2}$ (h)	54	46
p.o.		
Dose (mg/kg)	30	50
C_{max} (μmol/L)	2.2	5.7
t_{max} (h)	6.7	1.7
$AUC_{0\text{-}24}$ (μmol h/L)	34	58
F (%)	55	41

6727 in the ATP binding pocket of Plk1. The solvent-exposed basic benzamide-derived moiety of the compound was selected based on an extensive optimization program to further improve the pharmacokinetic properties of dihydropteridinones without changing the biochemical and cellular profile.[3]

Characterization of kinase specificity and cellular activity. BI 6727 potently inhibited Plk1 as well as the two closely related kinases Plk2 and Plk3 (IC_{50} values 0.87, 5, and 56 nmol/L, respectively). In contrast, assays using a panel of >50 other kinases (listed in ref. 19) failed to identify any inhibitory activity at concentrations up to 10 μmol/L.

BI 6727 inhibited proliferation of multiple cell lines derived from various cancer tissues, including carcinomas of the colon (HCT 116, EC_{50} = 23 nmol/L) and lung (NCI-H460, EC_{50} = 21 nmol/L), melanoma (BRO, EC_{50} = 11 nmol/L), and hematopoietic cancers (GRANTA-519, EC_{50} = 15 nmol/L; HL-60, EC_{50} = 32 nmol/L; THP-1, EC_{50} = 36 nmol/L and Raji, EC_{50} = 37 nmol/L) with EC_{50} values of 11 to 37 nmol/L. Representative dose-response curves for NCI-H460 and HCT 116 cells are shown in Fig. 1B. Immunofluorescence microscopy (Fig. 1C) and fluorescence-activated cell sorting analysis for DNA content (Fig. 2A and B) were used to analyze the cellular effects of BI 6727 in more detail. Immunofluorescence analysis of NCI-H460 cells treated for 24 hours with 100 nmol/L BI 6727 showed an accumulation of mitotic cells with monopolar spindles and positive staining for histone H3 phosphoserine 10 (Fig. 1C), confirming that cells are arrested early in the M phase. Consistent with these data, treatment of NCI-H460 cells with increasing concentrations of BI 6727 for 24 hours resulted in accumulation of cells with 4N DNA content (Fig. 2A), indicative of a cell cycle block in G_2-M phase, a phenotype expected for Plk1 inhibition (8). Starting at a concentration of 100 nmol/L, treated cells showed a prominent G_2-M peak in the fluorescence-activated cell sorting profile. Using this inhibitor concentration, a time course experiment was done (Fig. 2B). G_2-M arrest at 24 hours was followed by induction of apoptosis at 48 hours as shown by the increase in the sub-G_1 peak of the fluorescence-activated cell sorting profile. Induction of apoptosis was further confirmed by Western blot analysis of poly(ADP)ribose polymerase cleavage in NCI-H460 cells treated with 100 nmol/L BI 6727. Cleaved poly(ADP)ribose polymerase fragment was already detected after 24 hours of treatment; after 48 hours, all detectable poly(ADP)ribose polymerase protein had been converted to the fragment (Fig. 2C).

Pharmacokinetic profile of BI 6727. To determine the pharmacokinetic profile of BI 6727 in rodents (Fig. 2D), a single dose of 10 mg/kg was given as an i.v. 5-minute infusion to male Wistar rats (n = 4). Plasma concentrations of BI 6727 were measured at various time points after start of the infusion using a high-performance liquid chromatography/tandem mass spectrometry assay and various pharmacokinetic parameters were calculated (Table 1). The total plasma clearance was low at 8.9 mL/min/kg, corresponding to <20% of the hepatic blood flow. In contrast, the volume of distribution at the steady state (V_{ss}) was very high at 22 L/kg, indicating excellent tissue penetration. A similar experiment was done in mice (n = 3), giving 35 mg/kg BI 6727 i.v. (Fig. 2D; Table 1). Plasma clearance was low at 10 mL/min/kg corresponding to ~10% of the hepatic blood flow. Similar to rats, the V_{ss} was high at 7.6 L/kg. As part of our ADME analysis, we noted good oral bioavailability (F) of BI 6727 across species (mouse F = 41%, rat F = 55%, and dog F = 53%).

Efficacy of BI 6727 in human tumor xenograft models using i.v. and oral treatment schedules. We next investigated the ability of BI 6727 to inhibit growth of s.c. human carcinoma xenografts in nude mice. Consecutive cycles of treatment with BI 6727 given oral or i.v. for up to 6 weeks were efficacious in multiple xenograft models (Table 2). Treatment was well tolerated as judged by clinical signs and body weight changes (Fig. 3A and D and data not shown). Figure 3A and B shows results of experiments using the HCT 116 colon carcinoma model. We tested efficacy of BI 6727 after oral administration comparing three different administration schedules (once a week, twice a week, or daily; Fig. 3A). At a total weekly dose of 50 mg/kg, all treatment schedules showed comparable efficacy and were well tolerated. In the same model, i.v. administration of a daily dose of 15, 20, or 25 mg/kg on 2 consecutive days per week led to significant tumor growth delay and even tumor regression (Fig. 3B). Similar efficacy was observed in an independent experiment where 20 or 30 mg/kg BI 6727, respectively, were given i.v. once a week (Table 2). To test the efficacy of BI 6727 in a more rigorous setting, treatment of HCT 116 tumors was initiated when an average tumor size of ~400 mm^3 had been reached (Fig. 3C). Five cycles of 20 mg/kg BI 6727 given on 2 consecutive days per week resulted in tumor regression, whereas all vehicle-treated control animals showed progressive disease.

BI 6727 was also active in a non–small cell lung carcinoma xenograft model derived from NCI-H460 cells (Table 2). Oral doses of 70 mg/kg given once weekly or 10 mg/kg daily significantly delayed tumor growth (Table 2). Efficacy of BI 6727 was further studied in a model of taxane-resistant colon carcinoma (Fig. 3D). This model is based on serial transplantation of tumor fragments rather than inoculation of cultured cells, and the tissue architecture preserves typical features of human colon carcinoma. The efficacy of BI 6727 was compared with docetaxel in this model. Because docetaxel is given i.v. in clinical practice, we chose the i.v. administration route for both compounds. Whereas docetaxel given once a week at the

[3] Manuscript in preparation.

maximally tolerated dose (note progressive weight loss in Fig. 3D, *right*) did not show efficacy, 15 mg/kg BI 6727 given i.v. on 2 consecutive days significantly suppressed tumor growth and was well tolerated (Fig. 3D, *left* and *right*). In summary, BI 6727 shows efficacy in multiple xenograft models using i.v. or oral administration schedules (Table 2).

Using immunohistochemical methods, we were able to show that tumor response to treatment with BI 6727 is accompanied by an increase in the mitotic index as well as an increase in apoptosis (Fig. 4). HCT 116 tumor-bearing nude mice were injected with a single dose of 40 mg/kg BI 6727 or vehicle control and tumor tissue as well as pieces of the small and large intestines were removed 6, 24, and 48 hours after administration of BI 6727. The mitotic index was determined on frozen sections by staining with an antibody to histone H3 phosphoserine 10 (pH3), and apoptotic cells were visualized using a TUNEL assay. Twenty-four hours after administration of BI 6727, a significant (13-fold) increase in mitotic cells was observed in these tumors compared with tumors from control mice (Fig. 4A). Apoptotic cells in the BI 6727–treated tumors were detected as early as 24 hours after administration of BI 6727 and their number increased further at 48 hours (4.5-fold increase compared with control tumors; Fig. 4B and data not shown). In contrast, the mitotic index and the number of apoptotic cells did not increase in the small intestine and large intestine samples examined after treatment with a single dose of BI 6727 compared with samples from control animals (data not shown), suggesting that the proliferation rate of the intestinal cells is not high enough to be detectably affected by a single dose of BI 6727. Nevertheless, BI 6727 is expected to inhibit mitosis of all dividing cancer as well as normal cells, as reported for BI 2536 (19).

Drug exposure in tissues. To further evaluate tissue exposure and residence time of BI 6727 *in vivo*, which is likely more decisive for efficacy than plasma exposure, a single dose of 35 mg/kg BI 6727 was given i.v. to nude mice bearing s.c. xenografts of the human HCT 116 colon carcinoma. Tumors, multiple organs, as well as plasma samples were collected at various time points after compound administration, and the concentration of BI 6727 in tissue extracts was determined (Fig. 4C). Although exposure differences between organs—possibly reflecting different perfusion rates—were observed, overall a high tissue exposure was determined in these extracts, consistent with the high volume of distribution of BI 6727. Interestingly, drug concentrations in tumor tissue were much higher (a maximum of 32 μmol/L was reached 8 hours postadministration) than in plasma (7 μmol/L at 1 hour) and longer lasting. One hundred sixty-eight hours after administration, a concentration of 4 μmol/L was measured in the tumor, whereas plasma levels were only 8 nmol/L. Although it is clear that concentrations measured in the tissue extracts do not reflect free compound levels, the data suggest that tumor cells are efficiently exposed to BI 6727 *in vivo*.

Discussion

Targeting mitosis is an established approach for cancer therapy, and taxanes as well as *Vinca* alkaloids are currently used to treat a broad variety of cancer types. However, these drugs have significant limitations as they are ineffective for many cancer types and patients suffer from toxicities related to the broad requirement for microtubule function in critical cellular processes unrelated to mitosis. New mitosis-specific targets for cancer therapy have emerged in recent years, including the mitotic kinesins and the Plk and Aurora families of serine/threonine kinases, and a first wave of inhibitors are currently under evaluation in early clinical trials (33, 34). These novel antimitotic agents have the potential to provide similar or improved efficacy compared with microtubule-targeting agents combined with improved tolerability and are being explored to overcome primary and secondary resistance to these drugs.

The essential role of Plk1 during mitosis has been characterized in much detail (1). Although recent publications suggest additional physiologic roles for Plk1, i.e., in processes such as invasion, telomere stabilization, or the regulation of DNA topoisomerase IIα (35–37), the attractiveness of Plk1 as a target in all cancer cells irrespective of mutations in oncogenes or tumor suppressor genes, and therefore its potential relevance for cancer treatment across indications, remains high. In previous studies with BI 2536, we have opened up the evaluation of small-molecule kinase inhibitors to provide detailed insights into Plk1 function in cells and animal models and new options for cancer therapy (6, 13, 19). Like BI 2536, BI 6727 is an ATP-competitive kinase inhibitor from the dihydropteridinone class of compounds. Recently, additional chemical series providing inhibition of Plk1 have been

Table 2. Efficacy of BI 6727 in multiple xenograft models

Cell line	Daily dose (mg/kg)	Schedule	Route	Weekly dose (mg/kg/wk)	T/C (%)	Weekly AUC_{0-24} (μmol/L)
HCT 116	25	Twice a week	i.v.	50	0.3	75
	20	Twice a week	i.v.	40	1	66
	15	Twice a week	i.v.	30	1	37
HCT 116	20	Once a week	i.v.	20	9	40
	30	Once a week	i.v.	30	3	52
HCT 116	50	Once a week	p.o.	50	2	44
	25	Twice a week	p.o.	50	2	43
	7	Daily	p.o.	49	3	44
NCI-H460	70	Once a week	p.o.	70	20	58
	10	Daily	p.o.	70	6	61
CXB1	15	Twice a week	i.v.	30	12	nd

Abbreviations: T/C, treated versus control; nd, not determined.

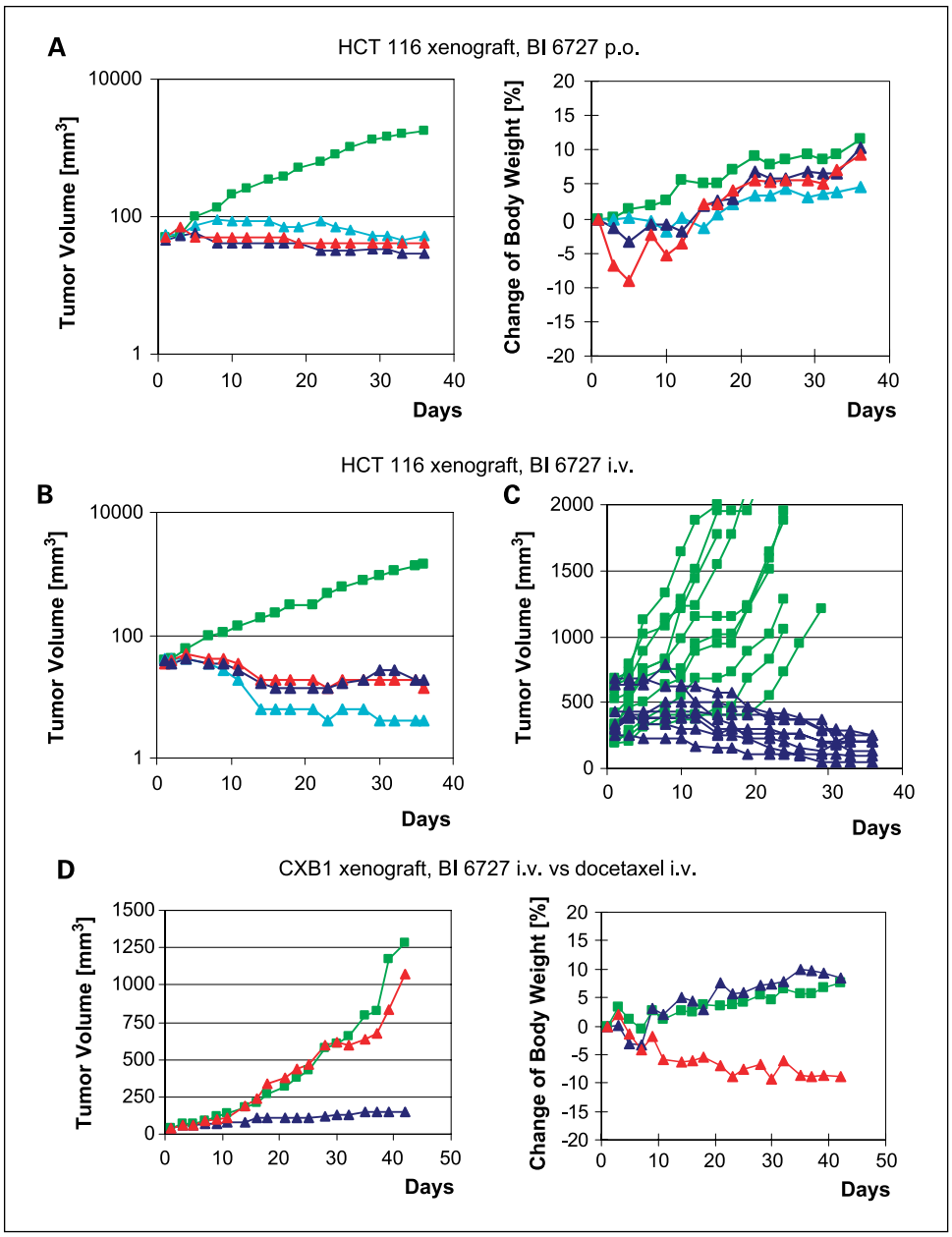

Fig. 3. Efficacy and tolerability of BI 6727 in human colon carcinoma xenograft models after oral or i.v. administration. *A,* nude mice bearing established HCT 116 human colon carcinoma tumors with an average size of ~50 to 80 mm^3 were treated orally for five cycles with either vehicle (*green squares*) or with BI 6727 once a week (*red triangles*), twice a week on consecutive days (*blue triangles*) or daily (*turquoise triangles*), administering in each treatment group a weekly dose of 50 mg/kg. Median tumor volumes of 10 animals average per treatment group (*left*) and body weight changes in percent of initial body weight (*right*). *B,* nude mice bearing established HCT 116 human colon carcinoma tumors with an average size of ~50 to 80 mm^3 were treated i.v. twice a week on consecutive days with either vehicle (*green squares*) or with doses of 15 mg/kg (*blue triangles*), 20 mg/kg (*red triangles*) or 25 mg/kg (*turquoise triangles*) BI 6727, respectively, for five cycles. Median tumor volumes of 10 animals per treatment group. *C,* nude mice bearing established HCT 116 human colon carcinoma tumors with an average size of ~400 mm^3 were treated i.v. twice a week on consecutive days with either vehicle (*green squares, n* = 10 animals per treatment group) or with 20 mg/kg BI 6727 (*blue triangles, n* = 8 animals per treatment group). Each graph shows the growth of an individual tumor. *D,* nude mice bearing established CXB1 human colon carcinoma tumors (average size ~50 mm^3) derived from patient material via serial transplantation were treated i.v. for six cycles twice a week on consecutive days with either vehicle (*green squares*) or 15 mg/kg BI 6727 (*blue triangles*). In addition, one treatment group received 15 mg/kg docetaxel i.v. once a week (*red triangles*). Median tumor volumes of 10 animals average per treatment group (*left*) and body weight changes in percent of initial body weight (*right*).

described (7, 27–29). BI 6727 potently inhibits Plk1 kinase activity (IC_{50} = 0.87 nmol/L) and the phenotype of cancer cells treated with BI 6727 over a wide concentration range is consistent with that induced by Plk1-specific siRNAi (8). At higher concentrations, BI 6727 also inhibits the related Polo-like kinase family members Plk2 and Plk3. Compared with Plk1, much less is known about the physiologic roles of these enzymes, and eventual consequences of inhibition of these enzymes in terms of efficacy and tolerability of drug candidates cannot currently be predicted. Whereas Plk1 transcripts are only expressed in proliferating cells, Plk2 and Plk3 transcripts show broad tissue distribution and are also expressed in postmitotic neurons (38). Plk2 may primarily function as a regulator of G_1- and early S-phase progression, of centriole duplication during the S phase, and may also play a role in the DNA damage checkpoint (17, 39–41). However, Plk2-deficient mouse embryonic fibroblasts show only subtle effects on cell cycle progression and Plk2-/- mice are viable, with embryos showing only slightly retarded overall growth and defects in skeletal development (42). Plk3 is a nucleolar protein; levels peak in the G_1 phase of the cell cycle and may regulate entry into the S phase (43, 44). Nevertheless, Plk3 is apparently not essential for cell cycle progression, as Plk3-/- mice do not show growth defects (45). Interestingly, Plk1 and Plk3 have recently been proposed as tumor suppressor genes based on the fact that Plk1+/- and Plk3-/- mice seem to develop tumors with somewhat increased frequency (45, 46).

In vitro tests with BI 6727 show promising activity against cells resistant to taxanes or *Vinca* alkaloids. Briefly, BI 6727 is able to inhibit the proliferation of NCI-H460 cells preselected for resistance to high concentrations of vincristine. Similar results were obtained with a melanoma cell line ectopically expressing the *MDR1* gene (BROmdr, data not shown), suggesting that BI 6727 is either less sensitive to these resistance

mechanisms than taxanes or *Vinca* alkaloids or that the high tissue permeability of BI 6727 may compensate for transporter-mediated drug efflux. Consistent with these *in vitro* observations, BI 6727 is highly efficacious not only in standard nude mouse xenograft models of human cancers but also in the taxane-resistant CXB1 xenograft model of colorectal cancer. We consider CXB1 to be particularly attractive for evaluation of drug resistance *in vivo* because it was neither genetically modified nor selected *in vitro* and shows histopathologic features much more akin to authentic human cancers than

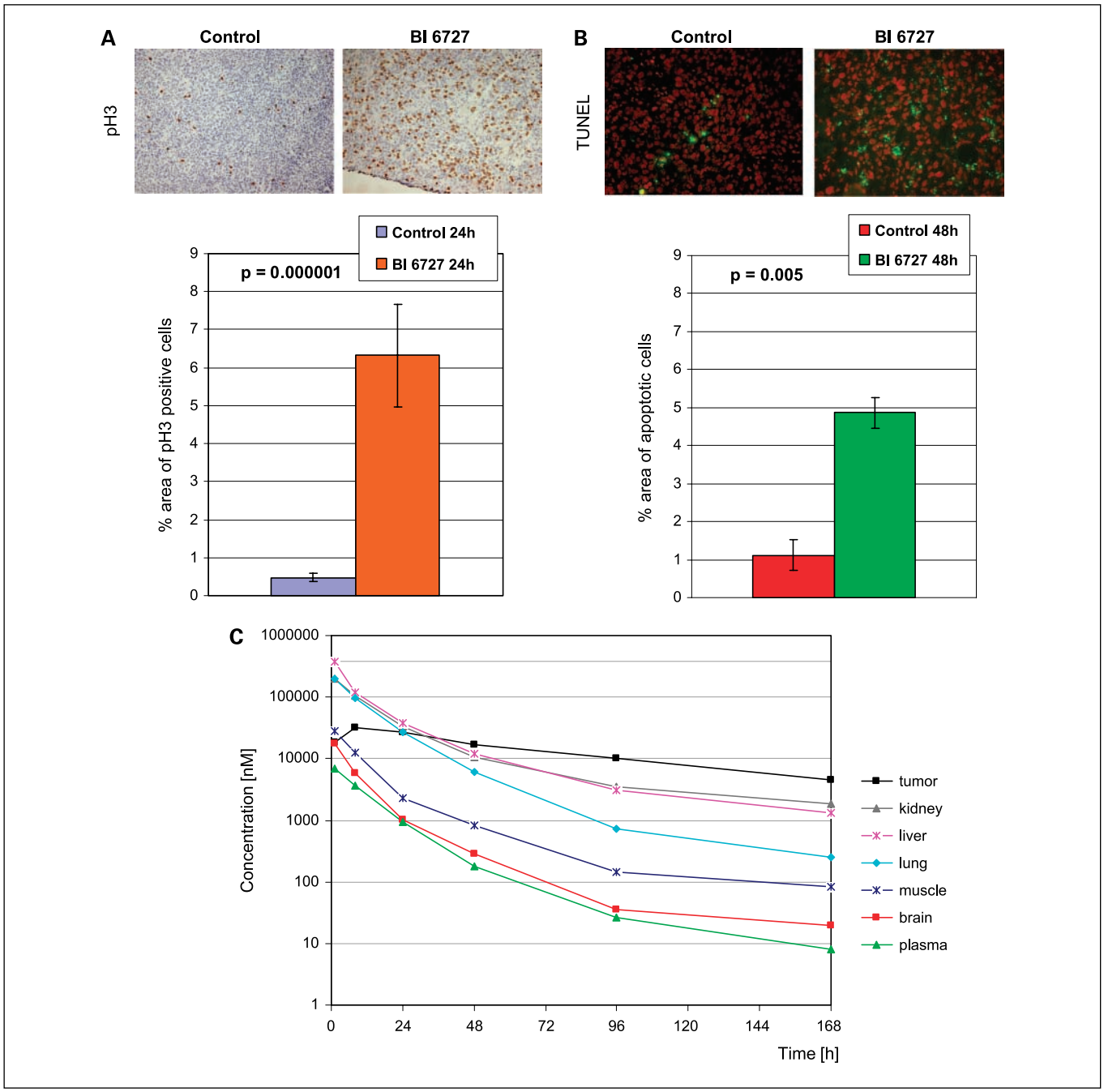

Fig. 4. Tissue exposure and induction of mitotic arrest and apoptosis *in vivo*. *A,* treatment with BI 6727 significantly increases the number of tumor cells arrested in mitosis. The mitotic index was determined by immunohistochemistry on frozen sections from control and BI 6727–treated animals 24 h after administration of the compound using an antibody to phospho-Ser[10] histone H3 (*pH3*; *top*). The bar graph (*bottom*) shows a comparison of the tumor cell area occupied by mitotic cells in control mice compared with BI 6727–treated mice using Definiens Developer image analysis software as described in Materials and Methods. Columns, median; bars, SD. Image analysis was done on three representative histologic fields (10×) from each of the three control and the three treated mice. *B,* BI 6727 induces apoptosis in tumor cells. Tumor samples from control and BI 6727–treated mice were analyzed by a TUNEL assay 48 h after administration of the compound or vehicle control (*top*). The bar graph (*bottom*) shows the increase in apoptotic cells in tumor samples from treated animals compared with tumor samples from control mice. Columns, median; bars, SD. Image analysis was done as above on three representative histologic fields (40×) from each of the two BI 6727–treated mice and the two control mice. *C,* nude mice bearing established subcutaneous HCT 116 tumors ($n = 3$ per time point) were treated i.v. with a single dose of 35 mg/kg BI 6727. Tumors, multiple organs (brain, kidney, liver, lung and muscle), and EDTA plasma samples were collected at various time points after administration of BI 6727 (1, 8, 24, 48, 96, and 168 h). BI 6727 concentrations were measured in plasma samples as well as in tissue extracts using high-performance liquid chromatography/tandem mass spectrometry methods.

typical cell line–derived models. Moreover, it represents a cancer model where MDR1/P-gp drug efflux pump expression in a polarized epithelial tissue (data not shown) may contribute to drug resistance in a pharmacologically relevant manner.

Our results in xenograft models suggest that BI 6727 is suitable for use in a wide range of treatment schedules. However, in the clinical context, the relevant tissue levels and notably levels of free versus protein-bound drug as well as exchange rates from bound to free drug are difficult to assess and cannot simply be extrapolated from plasma pharmacokinetics. In a pragmatic approach, we have prioritized BI 6727 for clinical development based on pharmacokinetic characteristics indicative of high and sustained exposure in tumor tissue. It is worth noting that early clinical studies of BI 6727 given by i.v. infusion to cancer patients seem to confirm the predicted high volume of distribution (>3,600 liters) and long half-life (about 110 hours; ref. 47). In addition, although it is too early to assess the effect of these distinctive pharmacokinetic properties on efficacy, the phase I results provide first evidence of antitumor activity as well as a favorable safety profile, with reversible hematotoxicity as the main side effect (47).

Disclosure of Potential Conflicts of Interest

No potential conflicts of interest were disclosed.

Acknowledgments

We thank the entire Plk1 Research and Development team for their contributions. All authors are employees of the Boehringer Ingelheim group of companies. We thank Proteros biostructures GmbH, Germany, for generating the cocrystal structure of Plk1 with BI 6727.

References

1. Petronczki M, Lenart P, Peters JM. Polo on the rise—from mitotic entry to cytokinesis with Plk1. Dev Cell 2008;14:646–59.
2. van Vugt MA, Medema RH. Getting in and out of mitosis with Polo-like kinase-1. Oncogene 2005;24:2844–59.
3. Toyoshima-Morimoto F, Taniguchi E, Shinya N, Iwamatsu A, Nishida E. Polo-like kinase 1 phosphorylates cyclin B1 and targets it to the nucleus during prophase. Nature 2001;410:215–20.
4. Lane HA, Nigg EA. Antibody microinjection reveals an essential role for human polo-like kinase 1 (Plk1) in the functional maturation of mitotic centrosomes. J Cell Biol 1996;135:1701–13.
5. Sumara I, Vorlaufer E, Stukenberg PT, et al. The dissociation of cohesin from chromosomes in prophase is regulated by Polo-like kinase. Mol Cell 2002;9:515–25.
6. Lenart P, Petronczki M, Steegmaier M, et al. The small-molecule inhibitor BI 2536 reveals novel insights into mitotic roles of polo-like kinase 1. Curr Biol 2007;17:304–15.
7. Santamaria A, Neef R, Eberspacher U, et al. Use of the novel Plk1 inhibitor ZK-thiazolidinone to elucidate functions of Plk1 in early and late stages of mitosis. Mol Biol Cell 2007;18:4024–36.
8. Sumara I, Gimenez-Abian JF, Gerlich D, et al. Roles of polo-like kinase 1 in the assembly of functional mitotic spindles. Curr Biol 2004;14:1712–22.
9. Eckerdt F, Strebhardt K. Polo-like kinase 1: target and regulator of anaphase-promoting complex/cyclosome-dependent proteolysis. Cancer Res 2006;66:6895–8.
10. Brennan IM, Peters U, Kapoor TM, Straight AF. Polo-like kinase controls vertebrate spindle elongation and cytokinesis. PLoS ONE 2007;2:e409.
11. Burkard ME, Randall CL, Larochelle S, et al. Chemical genetics reveals the requirement for Polo-like kinase 1 activity in positioning RhoA and triggering cytokinesis in human cells. Proc Natl Acad Sci U S A 2007;104:4383–8.
12. Randall CL, Burkard ME, Jallepalli PV. Polo kinase and cytokinesis initiation in mammalian cells: harnessing the awesome power of chemical genetics. Cell Cycle 2007;6:1713–7.
13. Petronczki M, Glotzer M, Kraut N, Peters JM. Polo-like kinase 1 triggers the initiation of cytokinesis in human cells by promoting recruitment of the RhoGEF Ect2 to the central spindle. Dev Cell 2007;12:713–25.
14. Smits VA, Klompmaker R, Arnaud L, Rijksen G, Nigg EA, Medema RH. Polo-like kinase-1 is a target of the DNA damage checkpoint. Nat Cell Biol 2000;2:672–6.
15. van Vugt MA, Smits VA, Klompmaker R, Medema RH. Inhibition of Polo-like kinase-1 by DNA damage occurs in an ATM- or ATR-dependent fashion. J Biol Chem 2001;276:41656–60.
16. van Vugt MA, Bras A, Medema RH. Polo-like kinase-1 controls recovery from a G_2 DNA damage-induced arrest in mammalian cells. Mol Cell 2004;15:799–811.
17. van de Weerdt BC, Medema RH. Polo-like kinases: a team in control of the division. Cell Cycle 2006;5:853–64.
18. Golsteyn RM, Mundt KE, Fry AM, Nigg EA. Cell cycle regulation of the activity and subcellular localization of Plk1, a human protein kinase implicated in mitotic spindle function. J Cell Biol 1995;129:1617–28.
19. Steegmaier M, Hoffmann M, Baum A, et al. BI 2536, a potent and selective inhibitor of polo-like kinase 1, inhibits tumor growth *in vivo*. Curr Biol 2007;17:316–22.
20. Takai N, Hamanaka R, Yoshimatsu J, Miyakawa I. Polo-like kinases (Plks) and cancer. Oncogene 2005;24:287–91.
21. Strebhardt K, Ullrich A. Targeting polo-like kinase 1 for cancer therapy. Nat Rev Cancer 2006;6:321–30.
22. Ismael GF, Rosa DD, Mano MS, Awada A. Novel cytotoxic drugs: old challenges, new solutions. Cancer Treat Rev 2008;34:81–91.
23. Bergnes G, Brejc K, Belmont L. Mitotic kinesins: prospects for antimitotic drug discovery. Curr Top Med Chem 2005;5:127–45.
24. Duhl DM, Renhowe PA. Inhibitors of kinesin motor proteins—research and clinical progress. Curr Opin Drug Discov Devel 2005;8:431–6.
25. de Carcer G, de Castro IP, Malumbres M. Targeting cell cycle kinases for cancer therapy. Curr Med Chem 2007;14:969–85.
26. Gautschi O, Heighway J, Mack PC, Purnell PR, Lara PN, Jr., Gandara DR. Aurora kinases as anticancer drug targets. Clin Cancer Res 2008;14:1639–48.
27. Lansing TJ, McConnell RT, Duckett DR, et al. *In vitro* biological activity of a novel small-molecule inhibitor of polo-like kinase 1. Mol Cancer Ther 2007;6:450–9.
28. McInnes C, Mazumdar A, Mezna M, et al. Inhibitors of Polo-like kinase reveal roles in spindle-pole maintenance. Nat Chem Biol 2006;2:608–17.
29. Peters U, Cherian J, Kim JH, Kwok BH, Kapoor TM. Probing cell-division phenotype space and Polo-like kinase function using small molecules. Nat Chem Biol 2006;2:618–26.
30. Gumireddy K, Reddy MV, Cosenza SC, et al. ON01910, a non-ATP-competitive small molecule inhibitor of Plk1, is a potent anticancer agent. Cancer Cell 2005;7:275–86.
31. Kothe M, Kohls D, Low S, et al. Structure of the catalytic domain of human polo-like kinase 1. Biochemistry 2007;46:5960–71.
32. Kothe M, Kohls D, Low S, et al. Selectivity-determining residues in Plk1. Chem Biol Drug Des 2007;70:540–6.
33. Jackson JR, Patrick DR, Dar MM, Huang PS. Targeted anti-mitotic therapies: can we improve on tubulin agents? Nat Rev Cancer 2007;7:107–17.
34. Schmidt M, Bastians H. Mitotic drug targets and the development of novel anti-mitotic anticancer drugs. Drug Resist Updat 2007;10:162–81.
35. Li H, Wang Y, Liu X. Plk1-dependent phosphorylation regulates functions of DNA topoisomerase IIα in cell cycle progression. J Biol Chem 2008;283:6209–21.
36. Rizki A, Mott JD, Bissell MJ. Polo-like kinase 1 is involved in invasion through extracellular matrix. Cancer Res 2007;67:11106–10.
37. Wu ZQ, Yang X, Weber G, Liu X. Plk1 phosphorylation of TRF1 is essential for its binding to telomeres. J Biol Chem 2008;283:25503–13.
38. Kauselmann G, Weiler M, Wulff P, et al. The polo-like protein kinases Fnk and Snk associate with a Ca(2+)- and integrin-binding protein and are regulated dynamically with synaptic plasticity. EMBO J 1999;18:5528–39.
39. Warnke S, Kemmler S, Hames RS, et al. Polo-like kinase-2 is required for centriole duplication in mammalian cells. Curr Biol 2004;14:1200–7.
40. Burns TF, Fei P, Scata KA, Dicker DT, El Deiry WS. Silencing of the novel p53 target gene Snk/Plk2 leads to mitotic catastrophe in paclitaxel (Taxol)-exposed cells. Mol Cell Biol 2003;23:5556–71.
41. Shimizu-Yoshida Y, Sugiyama K, Rogounovitch T, et al. Radiation-inducible hSNK gene is transcriptionally regulated by p53 binding homology element in human thyroid cells. Biochem Biophys Res Commun 2001;289:491–8.
42. Ma S, Charron J, Erikson RL. Role of Plk2 (Snk) in mouse development and cell proliferation. Mol Cell Biol 2003;23:6936–43.
43. Zimmerman WC, Erikson RL. Polo-like kinase 3 is required for entry into S phase. Proc Natl Acad Sci U S A 2007;104:1847–52.
44. Zimmerman WC, Erikson RL. Finding Plk3. Cell Cycle 2007;6:1314–8.
45. Yang Y, Bai J, Shen R, et al. Polo-like kinase 3 functions as a tumor suppressor and is a negative regulator of hypoxia-inducible factor-1 α under hypoxic conditions. Cancer Res 2008;68:4077–85.
46. Lu LY, Wood JL, Minter-Dykhouse K, et al. Polo-like kinase 1 is essential for early embryonic development and tumor suppression. Mol Cell Biol 2008;28:6870–6.
47. Schöffski P, Awada A, Dumez H, et al. A Phase I single dose escalation study of the novel Polo-like kinase 1 inhibitor BI 6727 in patients with advanced solid tumors. Eur J Cancer Suppl 2008;6:14–5.